Characterization of the THz radiation source at the Frascati linear accelerator

E. Chiadroni, M. Bellaveglia, P. Calvani, M. Castellano, L. Catani et al.

Related Articles

Additional information on Rev. Sci. Instrum.

Characterization of the THz radiation source at the Frascati linear accelerator

E. Chiadroni,[1] M. Bellaveglia,[1] P. Calvani,[2] M. Castellano,[1] L. Catani,[3,4] A. Cianchi,[3,4] G. Di Pirro,[1] M. Ferrario,[1] G. Gatti,[1] O. Limaj,[2] S. Lupi,[2,5] B. Marchetti,[3] A. Mostacci,[5,6] E. Pace,[1] L. Palumbo,[5,6] C. Ronsivalle,[7] R. Pompili,[1,3] and C. Vaccarezza[1]

[1]*INFN-LNF, Frascati, Italy*
[2]*Department of Physics, "La Sapienza" University of Rome, Rome, Italy*
[3]*Department of Physics, "Tor Vergata" University of Rome, Rome, Italy*
[4]*INFN Roma "Tor Vergata," Rome, Italy*
[5]*INFN Roma I, Rome, Italy*
[6]*Department of Basic and Applied Sciences for Engineering (SBAI), "Sapienza" University of Rome, Rome, Italy*
[7]*ENEA C.R. Frascati, Italy*

The linac driven coherent THz radiation source at the SPARC-LAB test facility is able to deliver broadband THz pulses with femtosecond shaping. In addition, high peak power, narrow spectral bandwidth THz radiation can be also generated, taking advantage of advanced electron beam manipulation techniques, able to generate an adjustable train of electron bunches with a sub-picosecond length and with sub-picosecond spacing. The paper reports on the manipulation, characterization, and transport of the electron beam in the bending line transporting the beam down to the THz station, where different coherent transition radiation spectra have been measured and studied with the aim to optimize the THz radiation performances. © *2013 American Institute of Physics.* [http://dx.doi.org/10.1063/1.4790429]

I. INTRODUCTION AND MOTIVATION

A growing interest in generating terahertz (THz) radiation is observed worldwide for both scientific and technological applications because of the peculiar characteristics of this radiation: it is non-ionizing, it penetrates dielectrics, it is highly absorbed by polar liquids, highly reflected by metals and reveals specific "fingerprint" absorption spectra arising from fundamental physical processes.

Both laser and accelerator-based THz sources are routinely implemented in several laboratories worldwide to optimize the emission features of the radiation in terms of spectral bandwidth, broadband, and narrowband, average and peak power, energy per pulse. Laser-based table-top THz sources present high average power and energy, because of the high repetition rate ($\approx$ kHz); they can also generate tunable THz radiation from photoconductive antennas and nonlinear media.[1] Short electron bunches are mandatory for the generation of highly performing accelerator-based THz sources, with high peak power, and broadband spectrum, extending up to a frequency given by the single electron bunch duration.

In order to achieve ps and sub-ps electron beams, different bunch compression techniques have been proposed[2,3] and successfully tested.[4,5] In III generation circular machines the low-momentum compaction, i.e., α-mode, has been successfully used at Bessy-II[6] and ANKA.[7] Short bunches can also be created by profiting from the bunch length energy dependence ($\sigma_z \approx E^{3/2}$), i.e., the bunch length can be reduced by lowering the machine energy. This compression scheme has been investigated, for instance, at Elettra.[8] In all cases, due to intrinsic magnetic optics limitation in a circular machine, only the ps-regime can be achieved providing a spectral coverage up to 1 THz. The sub-ps regime, corresponding to frequencies up to several THz, can be easily reached, instead, in linac-based machines. Indeed, these machines, recently developed for producing high brightness electron beams (HBEB) for Free-Electron Lasers (FELs) emission, are designed to work in the sub-ps regime down to $10-50$ fs.[9]

Linac-based coherent THz radiation from relativistic electron bunches is a potentially revolutionary source[10–12] in different field of science ranging from THz pump and probe experiments to molecular spectroscopy and imaging.[13] The study of ultra-fast and nonlinear phenomena can profit of peak electric fields greater than $1-10$ MV/cm[14] and intense single-cycle and multi-cycles THz radiation.[15]

So far the major limitation of accelerator-based sources was the lack of frequency tunability. Recently, it has been demonstrated that it is possible to generate tunable, narrowband, few-cycle, and multicycle coherent THz radiation by properly shaping the longitudinal charge distribution of the electron beam. Different approaches are currently used: a temporally shaped photocathode drive laser pulse,[16,17] a mask in a high dispersion, low beta function region of a beamline dogleg in order to produce a temporal bunch train out of a long bunch with a correlated energy spread,[18] a transversely segmented beam (with a multislit mask) manipulated via a transverse-to-longitudinal phase space exchange technique,[19] and an ultra-short relativistic electron bunch passing through a magnetic undulator.[20] For instance, molecular spectroscopy and imaging can benefit from a high peak power, tunable THz radiation with narrow spectral bandwidth.

Coherent THz radiation from relativistic ultra-short (sub-ps) electron bunches is commonly used also as powerful

longitudinal diagnostics in linac-drive FELs,[21] as presently done at Sources for Plasma Accelerators and Radiation Compton with Lasers and Beams (SPARC-LAB), or plasma-based accelerators,[22] which is an approved project at SPARC-LAB.

The generation of THz radiation at SPARC-LAB relies on the usage of sub-ps high brightness electron bunches when a broadband radiation is needed, while for tunable narrow-band radiation longitudinally modulated electron beams are produced and characterized. The production of a pulse train with sub-picosecond length and adjustable (sub)-picosecond inter-distance is itself very interesting due to its wide spectrum of other applications such as coherent excitation of plasma waves in plasma accelerators or ultrafast pump-probe FEL experiments.[23]

In this paper, we will resume the main results achieved at SPARC-LAB in the generation of THz radiation, as Coherent Transition Radiation (CTR), relying on the peculiar possibility of manipulating ultra-short (sub-ps) high-brightness electron beams and longitudinally modulated ones.[24] The technique used at SPARC-LAB to produce high brightness longitudinally compressed beams relies on low energy RF compression, named as velocity bunching.[4,5] Beyond the shorter bunch length, the velocity bunching technique is characterized by a longitudinal phase space distortion, leading to asymmetric current profiles which are responsible of the emission at higher frequencies thanks to the sharp rising charge distribution at the bunch head.

Longitudinally modulated electron beams are generated by properly shaping trains of UV laser pulses illuminating the metallic photocathode, in the RF gun followed by the RF compressor, i.e., the first linac section, operating in over-compression regime or by a magnetic compressor with R_{56} < 0: downstream the photoinjector the initial density modulation is converted, due to longitudinal space charge forces, in energy modulation, that after compression is transformed back to density modulation. The train characteristics, i.e., charge, length, and inter-distance, are completely controlled by the accelerator parameters with no particle losses, giving the possibility to produce high charge pulse trains. This technique is known as comb laser beam.

The paper focuses also on the main issues concerning the optimization of the THz radiation source giving some insight into the beam dynamics of a two and four bunches comb beam through the dogleg beamline. Start-to-end simulations have been used to both guide the operation and analyze experimental data.

II. THE SPARC-LAB TEST FACILITY

SPARC-LAB is a test facility based on the unique combination of high brightness electron beams, from the SPARC photoinjector,[25,26] with high intensity ultra-short laser pulses, from FLAME.[27] The joint presence of these two systems will allow the investigation of different configurations of plasma acceleration, i.e., self- and external-injection, laser and particle beam driven, and the development of a wide spectrum inter-disciplinary leading-edge research activity based on advanced radiation sources, e.g., coherent monochromatic X-ray
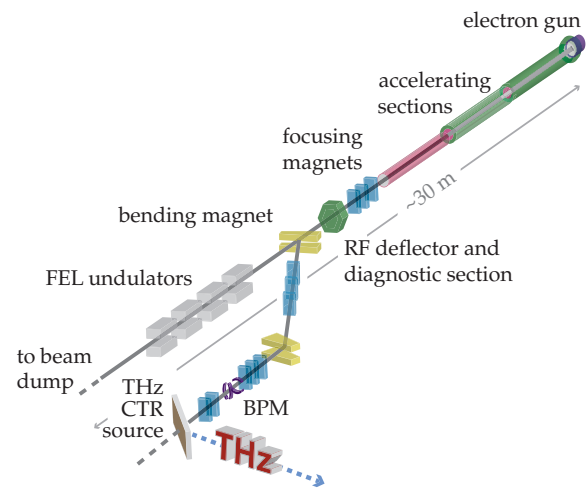

FIG. 1. SPARC schematic layout with the THz source placed at the end of the by-pass line.

and high peak power THz radiation, both broadband and narrowband.

The photoinjector is composed by a BNL/UCLA/SLAC type gun, operating at S-band (2.856 GHz) with high peak field (120 MV/m) on the incorporated metallic photocathode (Cu), generating a 5.6 MeV electron beam. The gun is then followed by three traveling wave (TW) sections whose accelerating gradient boosts the beam energy up to 180 MeV. The first one is also used as RF compressor (velocity bunching regime) by varying the beam injection phase. Solenoid coils embedding the first two sections can be powered to provide additional magnetic focusing to better control the beam envelope and the emittance oscillations under RF compression. A diagnostics transfer line allows to fully characterize the accelerated beam by measuring transverse emittance,[28] longitudinal profile, and slice emittance through a Radio-Frequency Deflector (RFD).[29] When SPARC is not operated in the FEL mode, the beam is bent by dipole magnets either by 14° towards the first dogleg beamline or by 25° towards the new beamlines for plasma acceleration and Thomson back-scattering. Figure 1 depicts a sketch of the layout, showing the SPARC linac and the first beamline, where the THz station is placed together with complementary experimental devices, i.e., a novel cavity beam position monitor and an electro-optical sampling apparatus.

Nowadays the SPARC-LAB scientific program ranges from advanced beam dynamics experiments,[5,24,30] devoted to beam physics understanding, advanced radiation generation, i.e. THz,[31–33] Compton, etc., to novel schemes for generation of FEL radiation,[34–37] to plasma acceleration experiments.[38,39]

In the following, we will focus on the activity concerning the generation, characterization and transport of both a high brightness single pulse electron beam and a multi-pulses train through the dogleg beamline down to the THz station, for the development of high peak power, both broadband and narrowband THz radiation, whose experimental layout is described in Sec. II A.

A. THz source experimental layout

The THz source is placed at the end of the dogleg beam-line, where CTR is generated at the interface of an aluminum coated silicon screen (30 × 30 mm size), placed in the vacuum pipe (60 mm diameter) at 45° with respect to the electron beam direction. The backward CTR radiation, reflected normally to the beam direction, is extracted through a crystalline z-cut quartz window (63 mm clear aperture) and propagated in air. The distance between the target and the vacuum window is 70 mm; therefore, the angular acceptance of the window is much greater than the natural opening angle ($\vartheta \approx 1/\gamma \approx 5$ mrad with $\gamma = 196$). A 152 mm focal length 90° off-axis parabolic mirror, whose focal plane corresponds to the source plane, parallelizes and reflects vertically the radiation beam down towards an aluminum flat mirror, placed at 45° with respect to the horizontal plane (Fig. 2, top). Frequency domain measurements[32] can be performed by means of either a Martin-Puplett interferometer[40] or bandpass mesh filters,[41] depending on the position of the first flat mirror in Fig. 2, bottom).

In the case of autocorrelation measurements, the radiation enters the first polarizer, whose wires are vertical to select horizontal polarization. The horizontally polarized transmitted radiation first reaches the beam splitter (BS), placed at 45°, whose wires are at 45° to the horizontal plane when viewed along the beam input axis. The BS divides the input signal into two equal, orthogonally polarized components, one being reflected towards the stationary roof mirror and the other being transmitted to the movable one, whose maximum travel distance is 36.7 mm with a minimum step width less than 1 μm. Radiation coming back from both arms to the beam splitter recombines, being then focused by a 90° off-axis parabolic mirror onto the detectors via the analyzing wiregrid,
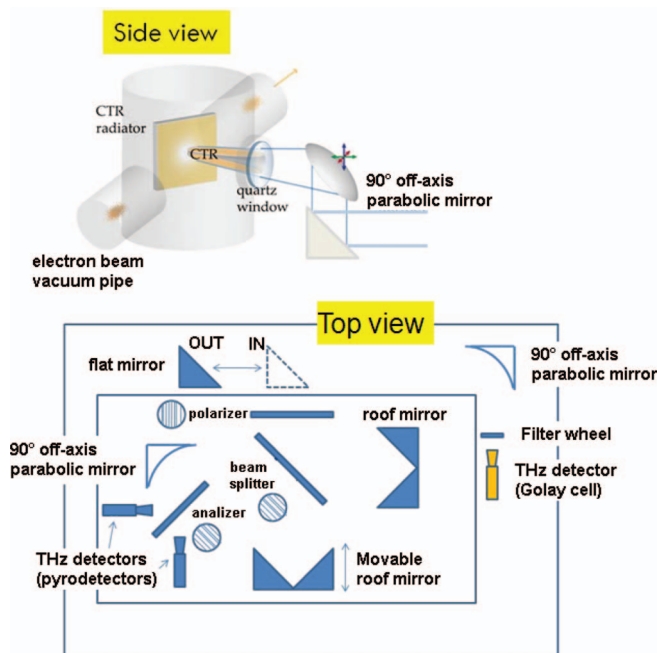

FIG. 2. Experimental layout for extraction (top) and detection (bottom) of THz radiation.
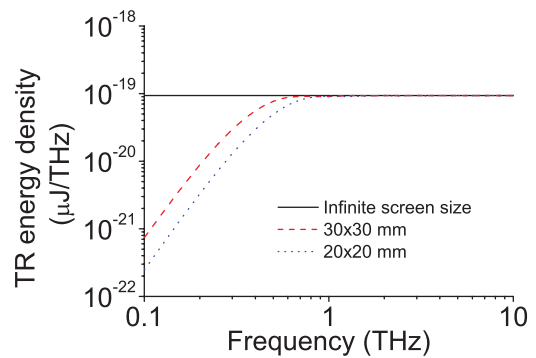

FIG. 3. Single electron TR energy density calculated for 100 MeV energy in case of an infinite screen (solid black line), in comparison with a 30 × 30 mm (dashed red line) and a 20 × 20 mm (dotted blue line) target.

located between the mirror and the detectors. Wire grids are wound from 10 μm diameter thick tungsten wire with a spacing of 20 μm. Either pyroelectric or Golay cell detectors, operating in a spectral range of 0.1–10 THz, can be used. Due to the finite size of the screen and optics acceptance, the CTR spectrum has a low frequency cut off, which can be evaluated as the frequency for which the Ginzburg-Frank formula is reduced by e^{-1}, i.e., 300 GHz (see Fig. 3). At high frequency, the quartz window transmission sets a limit at 5 THz.

III. THEORETICAL BACKGROUND

THz radiation is electromagnetic radiation whose frequency lies between the microwave and infrared regions of the spectrum. In linear accelerators broadband THz radiation is generated as coherent radiation emitted by sub-ps duration single electron bunches. THz radiation with narrow spectral bandwidth is, instead, produced by means of multi-bunches trains with THz scale spacing. In this section, we will discuss the generation of coherent radiation and the beam manipulation methods applied to enhance the THz radiation performances in terms of spectral bandwidth, peak power, and energy per pulse.

A. Coherent transition radiation

The emission mechanism considered here is Transition Radiation (TR) as produced when a relativistic charged particle crosses the interface between two media of different dielectric properties. The TR process was calculated analytically by Ginzburg and Frank[42] (GF) by solving the Maxwell equations in the assumptions of infinite size target, infinitely thin and ideally flat, perfectly conducting material and far-field approximation. The spectral angular distribution for a single electron is then described by the formula

$$\frac{d^2 I_{GF,sp}}{d\omega d\Omega} = \frac{e_0^2}{4\pi^3 \varepsilon_0 c} \frac{\beta^2 \sin \vartheta^2}{(1 - \beta^2 \cos \vartheta^2)^2}, \quad (1)$$

with c the speed of light, e_0 the charge of an electron, β the ratio of the velocity of the particle to the velocity of light, and ϑ the observation angle measured with respect to the backward direction. For frequencies well below the plasma frequency of the conduction electrons of the metal and in the limits

of validity of the GF formula (Eq. (1)), the spectral angular distribution of TR radiation does not present any dependence on the radiation frequency. However, in most practical cases the assumptions of infinite size target and far-field approximation are not completely fulfilled.[43] Indeed, for high electron energy and large emitted wavelength, the natural extent of the particle field, i.e., $\gamma\lambda/2\pi$, may exceed the dimension of the screen, causing the spectrum be a complicate function of beam energy, target extension, frequency, and angle of emission. As a consequence, the ideal GF formula (Eq. (1)) is not valid anymore and it must be replaced by the generalized one.[44] The effect on the TR spectrum is a strong suppression of the low frequencies side, as shown in Fig. 3. Figure 3 presents the single electron TR energy density calculated for 100 MeV energy in case of an infinite screen (solid black line), in comparison with a 30×30 mm (dashed red line) and a 20×20 mm (dotted blue line) target.

TR has the tendency to propagate in two main directions along the trajectory of the particle, in the forward direction (forward transition radiation, FTR) and in the backward direction (backward transition radiation, BTR), within a cone whose axis is coincident with the direction of propagation of the particle and with angular aperture proportional to $1/\gamma$, where γ is the Lorentz factor. In case the target is oriented with angle θ_0 with respect to the direction of the incident particle, the backward radiation propagates in the direction of the mirror reflection. From the experimental point of view, the $\theta_0 = 45°$ geometry is the most suitable one because the emitted radiation is well separated from the electron beam. The theoretical model, depicted by the GF formula, exactly describes the TR angular distribution in case the particle intersects the target surface normally. However, for relativistic electron beam energy, $\gamma \gg 1$, the GF formula can describe as well the TR angular distribution also in case of oblique incidence.[45]

When considering a bunch of charged particles with a finite size in both transverse and longitudinal dimensions, each particle in the bunch emits a radiation field with the same amplitude. The relative phase, instead, depends on the position within the bunch and on the direction of the radiation. The spectral angular distribution produced by a relativistic electron beam can be written as[46]

$$\frac{d^2I}{d\omega d\Omega} = \frac{d^2I_{sp}}{d\omega d\Omega}[N + N(N-1)F(\omega)], \qquad (2)$$

with $\omega = 2\pi c/\lambda$ the angular frequency of the emitted light, N the number of electrons in the bunch, and $\frac{d^2I_{sp}}{d\omega d\Omega}$ the generalized GF formula.[44] Under general conditions, $F(\omega)$ is the so-called three-dimensional (3D) bunch form factor,[47] defined as the square of the Fourier transform of the normalized particle distribution within the bunch, $S(\vec{r})$,

$$F(\omega) = \left| \int_V S(\vec{r}) e^{-i\frac{\omega}{c}\hat{n}\cdot\vec{r}} d\vec{r} \right|^2, \qquad (3)$$

$\hat{n}$ is the unit vector towards the observation point, and the integral is performed over the bunch volume V.[48,49] Two terms contribute to the total intensity (Eq. (2)): the first one, proportional to the number of particles, N, is the total intensity if the particles radiate all incoherently, each behaving independently one from the other; the second one dominates for short bunches when the N particles can be treated as a single macroparticle. All particles emit their radiation at the same phase coherently which means that the field amplitudes add with constructive interference and the intensity scales quadratically with the number of electrons per bunch, i.e., N^2.

From the definition of the 3D form factor (Eq. (3)), it results that the finite transverse size of the bunch can also affect the coherent amplification at short wavelengths and reduce the magnitude of the form factor, resulting in a narrower spectrum. The phase $\phi = \frac{\omega}{c}\hat{n}\cdot\vec{r}$ in Eq. (3) can be written, in cylindrical coordinates, as $\phi = \frac{\omega}{c}(\rho\sin\vartheta + z)$, ρ being the beam radius and z the longitudinal coordinate with respect to the bunch center of mass. As a consequence, at small observation angles, typical for radiation from highly relativistic electrons, and/or for finely collimated beams, the bunch transverse form factor has a weak influence on the coherent radiation spectrum.[50] In the following, we refer to $F(\omega)$, defined by

$$F(\omega) = \left| \int S(z) e^{-i\frac{\omega}{c}z} dz \right|^2, \qquad (4)$$

as the bunch longitudinal form factor, the contribution of the transverse one being negligible, as demonstrated in Fig. 4. Figure 4 demonstrates that even for acceptance angles larger than the natural opening angle of TR, i.e., $\vartheta \approx 1/\gamma$, the transverse form factor affects mainly the high frequency side of the spectrum in case of beam radius much larger than the longitudinal dimension.

From the point of view of THz radiation production, the N^2 dependency of coherent radiation results in a huge intensity gain with respect to most existing THz sources. Furthermore, since the bunch longitudinal form factor (Eq. (4)) is typically different from zero for wavelengths of the order, or longer than the bunch length, $\sigma_z = c\sigma_t$, it is clear that the coherent radiation spectrum can be extended towards high frequencies, i.e., several tens of THz, by acting on the bunch longitudinal dimension.
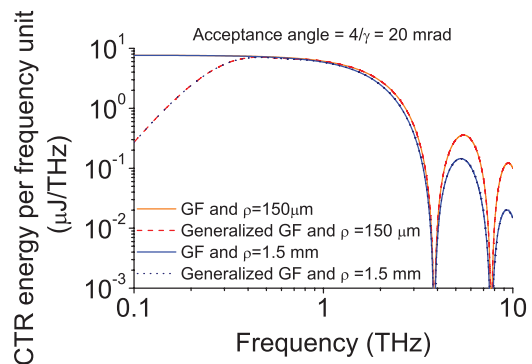

FIG. 4. Calculated CTR energy density for a 20 mrad acceptance angle, taking into account the 3D form factor for uniform distributed beams, both transversely and longitudinally. A 260 pC charge, 260 fs pulse duration and 100 MeV energy beam is considered. Orange and blue solid curves are obtained through the ideal GF formula, considering a 150 μm and 1.5 mm beam radius, respectively. The red dashed and the navy dotted curves take into account the target screen size, for a transverse beam radius of 150 μm and 1.5 mm, respectively.

B. Broadband generation

Short electron bunches are therefore mandatory for the generation of high peak THz power. Both magnetic and RF compression techniques can be used. In magnetic compressors, a bunch with a time-energy correlation (or chirp) is driven along an energy-dependent path length by a dispersive, non-isochronous beam transport section. While this scheme has been proved successful in increasing the beam current, the emittance growth due to coherent synchrotron radiation in bending magnets can be dramatic. As alternative, the compression scheme used at SPARC-LAB exploits the interaction with the electromagnetic fields of an accelerating cavity. Based on RF compression, it uses rectilinear trajectories, avoiding the damage suffered by the beam going through bending trajectories. This scheme is commonly known as "velocity bunching"[4] (VB).

The VB method is based on a time-velocity correlation in an electron bunch, causing electrons in the bunch tail to be faster than electrons in the bunch head. The correlated chirp induces a longitudinal phase space rotation in the traveling RF wave potential (longitudinal focusing) accelerating the beam inside a long multi-cell RF structure. Thus simultaneously, an off crest energy chirp is applied to the injected beam. If the beam is slightly slower than the phase velocity of the RF wave, when injected at the zero crossing field phase, it slips back to phases where the field is accelerating and, simultaneously, it is chirped and compressed. Therefore, compression and acceleration take place at the same time within the same accelerating section, i.e., the first one following the gun. An additional advantage is given by the fact that this compression section can be integrated in the emittance compensation scheme.[30] Indeed, the VB technique is characterized by longitudinal and transverse phase space distortions, leading to asymmetric current profiles, and higher final projected emittances, which can be however minimized by keeping the transverse beam size under control through solenoidal magnetic field in the region where the bunch is undergoing compression and the electron density increasing.[5] The asymmetric longitudinal profiles are instead responsible of the emission at higher frequencies thanks to the sharp rising charge distribution at the bunch head. Indeed, beyond the bunch longitudinal dimension, the longitudinal bunch shape has also a significant impact on the emission spectral content, as shown in Fig. 5, where the longitudinal bunch form factors for three different particle distributions, Gaussian (black solid line), uniform (red dashed line), and triangular (blue dotted line), with the same RMS bunch length, are depicted. The triangular-like longitudinal profile is then the most recommended to generate THz radiation extending up to higher frequencies.

C. Narrowband generation

Narrow spectral bandwidth and tunable THz radiation can be produced by a train of sub-ps electron bunches. An active method for tailoring an adjustable train of electron bunches with a sub-picosecond length with sub-picosecond spacing has been demonstrated at the SPARC-LAB test facility, combining the velocity bunching regime, and properly shaped trains of UV laser pulses hitting the photocathode (comb laser beam).[24,51]

The technique used to generate laser comb pulses relies on a birefringent crystal, where the input pulse is decomposed in two orthogonally polarized pulses with a time separation proportional to the crystal length. If more birefringent glasses are inserted in the laser beam path, it is possible to produce multi-peaks. A comb laser pulse illuminating a metallic photocathode in a RF gun generates a train of short electron bunches. Downstream the photoinjector, the beam acquires an energy modulation because of the space charge effects and, if injected in a RF-compressor operating in the over-compression regime, the energy modulation can be transformed back into a density modulation.[51] The train parameters, bunch charge, length, and inter-distance, are completely controlled by the accelerator with no particle losses. As a train of sub-ps relativistic electron bunches crosses an aluminum screen, coherent THz radiation is generated and its spectrum results in a series of narrow pulses whose THz central frequency and bandwidth depend on the bunches inter-distance and width. Figure 6 (left plot) shows the longitudinal profile of both a single bunch (red dashed line) and a four-bunches train with different time separation (blue solid and black dashed-dotted lines); the form factor of such longitudinal distributions is shown in Fig. 6 (right plot), highlighting the impact of the beam parameters on the THz emission.
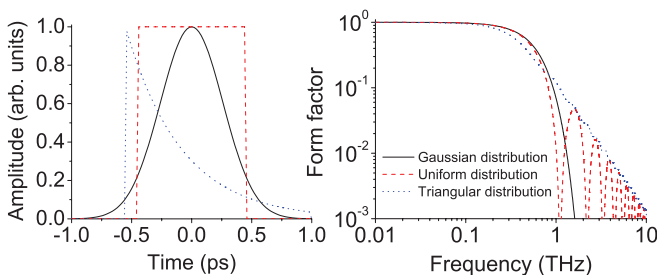

FIG. 5. Comparison of different longitudinal bunch distributions (left) and corresponding form factors (right) for the same RMS pulse duration, i.e., 0.26 ps, to highlight the impact of the longitudinal shape beyond the bunch length.
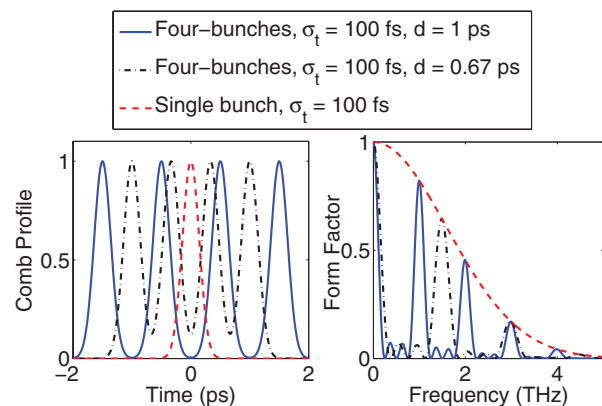

FIG. 6. (Left) Calculated four-pulses comb train with 1 ps pulse separation and 100 fs rms sub-pulse length (blue solid line), same sub-pulse length, but shorter inter-distance (black dashed-dotted line) and single bunch (red dashed line). (Right) Corresponding form factors.

Figure 6 also shows how the emission frequency can be tuned by changing the distance between pulses in the train. Therefore, combining the VB technique and a comb-like electron beam distribution, a tunable narrowband THz source can be produced.

Being the longitudinal distribution produced directly by a proper laser shaping, the method presented here does not foresee any reduction of the bunch charge; therefore, the coherent THz emission can take advantage of high charge pulse trains.

The main critical points consist in the high phase stability requirements and the need to control the emittance of a space charge dominated comb beam at low energy when the RF compressor is used.

In Secs. IV B 1 and IV B 2, we discuss the generation and the transverse and longitudinal phase space characterization of both a two-bunches and a four-bunches train, respectively. However, we will first discuss in Sec. III D the impact of the dogleg beamline on the preservation of well separated sub-bunches down to the THz station, affecting the broadening of the THz radiation spectral bandwidth.

D. Dogleg longitudinal dynamics

The longitudinal phase space evolution in the dogleg is dominated by nonlinearities given by high order chromatic terms.[52] Running the beam off-energy with a momentum $\widetilde{p}$ differing from the central momentum p_0 of the design trajectory, the beam centroid follows the trajectory of an off-momentum particle whose momentum dispersion is $\Delta = (\widetilde{p} - p_0)/p_0$. A particle with arbitrary momentum p then has the momentum error $\widetilde{\delta} = (p - \widetilde{p})/\widetilde{p}$ relative to the central momentum of the beam and the momentum error $\delta = (p - p_0)/p_0$ relative to the design momentum for which the beam line is optimized. The longitudinal transport pa-

rameters relative to the displaced momentum error $\widetilde{\delta}$ can be written as

$$z_f = z_0 + \widetilde{Q_5} + \widetilde{R_{56}}\widetilde{\delta} + \widetilde{T_{566}}\widetilde{\delta}^2 \text{ where } \widetilde{T_{566}} = T_{566}(\widetilde{p}/p_0)^2,$$

$$\widetilde{R_{56}} = \frac{\widetilde{p}}{p_0}(R_{56} + 2T_{566}\Delta) \text{ and } \widetilde{Q_5} = R_{56}\Delta + T_{566}\Delta^2$$

and are function of the momentum error Δ from the beam centroid, i.e., the difference between the actual energy and the design one. z_0 is the designed longitudinal position; additional details of the derivation and the notation used here are explained in Ref. 52.

In a comb beam, we can define the previous quantities for the whole beam and also for each sub-bunch in the train, meaning that any sub-bunch may undergo a longitudinal evolution different from the others.

For example, typical values for SPARC dogleg line are $R_{56} = -5$ mm with a $T_{566} = -95$ cm with a momentum spread which may be about few %; therefore, the $\widetilde{R_{56}}$ (the so called "effective" R_{56}) may also change sign within the bunch train itself, depending on the sub-bunch energy.

Such a nonlinear behavior is very important, since the dogleg acts as a compressor, i.e., modifying further the bunch train length, sub-bunches current and bunch separation, affecting THz emission. An example is shown in Fig. 7 for the longitudinal phase space of a four-bunches beam both at the exit of the linac (where the SPARC RFD-based longitudinal beam diagnostics is) and at the end of the dogleg (where a THz radiation-based longitudinal diagnostics is also present).

At the linac exit the four pulses are well separated (left plots). The right plots refer to a dogleg line with the quadrupoles set to have $R_{56} = -5$ mm with an energy 1 MeV lower than the energy at which the dogleg is optimized. The longitudinal phase space is completely distorted and the bunch profile has a modulation depth much worse, resulting
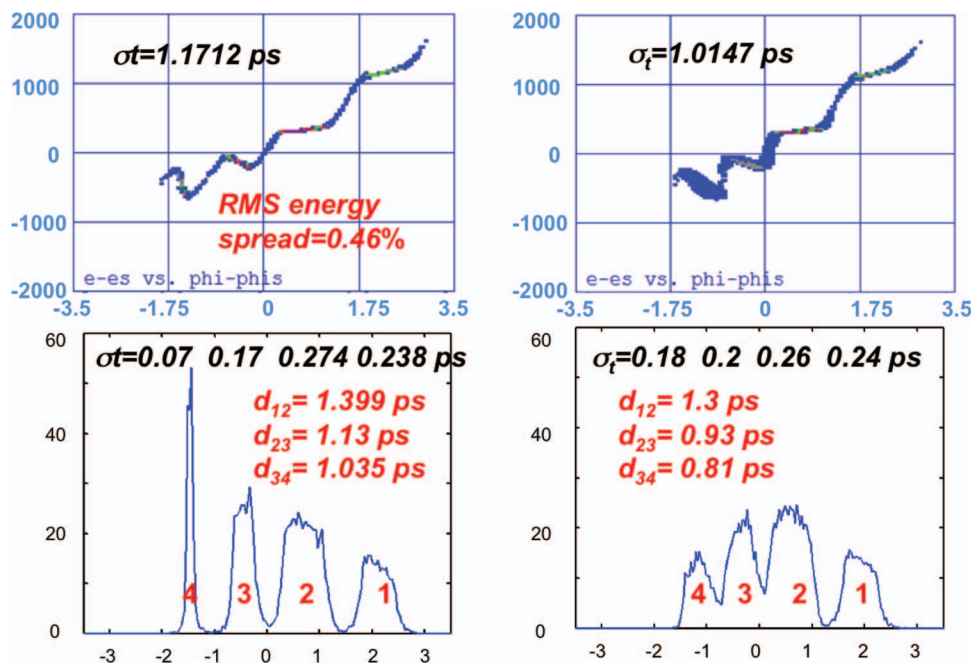

FIG. 7. Longitudinal phase space and current profile at the Linac exit (left plot) and at the THz station (right plots) (TSTEP simulation[53]).
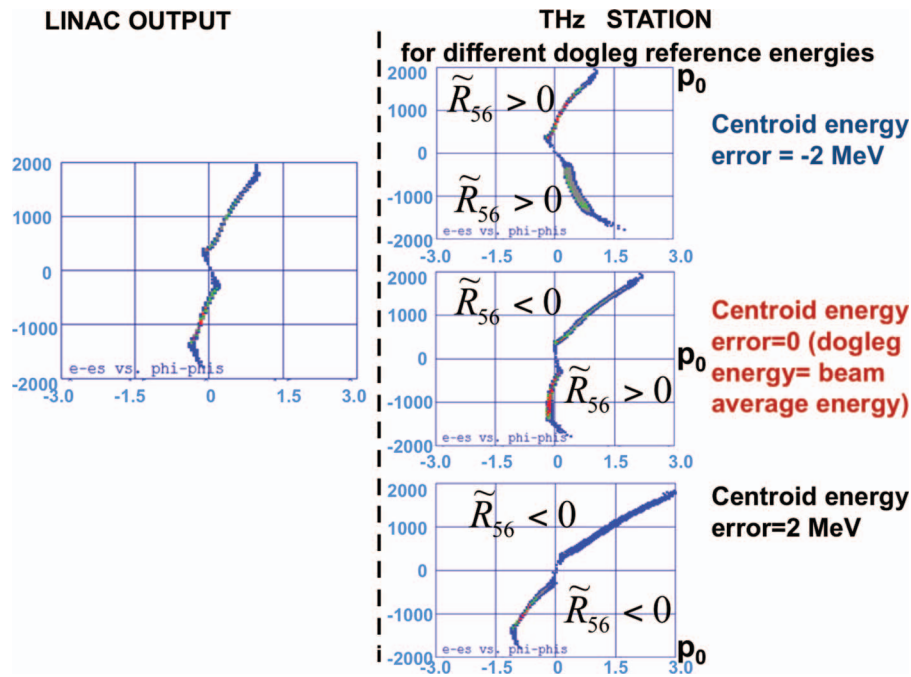
FIG. 8. Longitudinal phase space transport in the dogleg for a two bunches train. (Left plot) linac output; (right plots) THz station at the end of the dogleg. Due to high order chromatics effect in the dogleg and possible off energy operation, each bunch in the train may undergo different chirp, causing a degradation of the longitudinal modulation.

in a poor narrowband THz emitted radiation. Figure 7 shows TSTEP[53] simulation with a very detailed SPARC model and the resulting THz spectra are compatible with the measured ones.

Such high order chromatics effect (due to $T_{566} \gg R_{56}$) and possible off energy operation affects the longitudinal phase space transport in the dogleg even more for a two bunches comb beam which exhibits typically a higher energy spread. For example, it may result, for a two sub-bunches beam, in one sub-bunch lengthening, while the other is compressing, as confirmed also by simulations shown in Fig. 8. A similar behavior has been also observed in the experiment as presented in Sec. IV B 1.

E. Frequency-domain technique for the characterization of longitudinal distributions

The coherent spectrum of radiation emitted by both a sub-ps single bunch and a multi-bunches train can be retrieved by means of Fourier transform spectroscopy, based on the fact that the interference pattern (i.e., the interferogram) from a two beams interferometer is the Fourier transform of the radiation passing through it. In particular, for millimeter and sub-millimeter radiation a Martin-Puplett interferometer[40] is usually considered. The beam splitter is a polarizing grid, whose wires are at 45° with respect to the horizontal plane when viewed along the beam axis. The grid reflects the field with polarization parallel to the wires and transmits the orthogonal one. The roof mirrors rotate the polarization of the incident field upon reflection so that the radiation first transmitted by the grid is reflected when it returns, and vice versa. The reflected and transmitted components recombine then to produce a total field, at the analyzer grid which splits polar-

ization again into two components, parallel and orthogonal to the wires, whose intensity is detected by the THz detectors. The horizontal and vertical components are 90° out of phase and the amplitudes depend on the phase difference, $\omega\tau$, resulting in an elliptically polarized radiation; τ is the optical path difference. Assuming a source with an arbitrary intensity distribution, $I(\omega)$, the intensity of the recombined radiation at the detectors can be written as

$$V_{h,v} = \int_0^\infty I(\omega) \begin{cases} \cos^2\left(\frac{2\omega\tau}{2}\right) \\ \sin^2\left(\frac{2\omega\tau}{2}\right) \end{cases} d\omega. \qquad (5)$$

The normalized difference interferogram then can be written as $\delta(\tau) = \frac{V_h(\tau)-V_v(\tau)}{V_h(\tau)+V_v(\tau)}$, which corresponds to the Fourier transform of the radiation spectrum and it is the measured quantity.

For a longitudinally modulated beam the interferogram shows $2n - 1$ peaks, with n the number of bunches in the train. Let us consider a 4 sub-pulses radiation pulse, generated by a 4 sub-bunches electron beam. At zero optical path distance each sub-pulse within the two comb trains completely overlap, resulting in the maximum in the difference interferogram. As the path difference increases, the interferogram intensity decreases until three of the four pulses overlap, corresponding to the first side maxima. Increasing the distance, the interferogram intensity decreases again until only two of the sub-pulses super-impose, giving the second side maxima, smaller than the previous ones. Finally, as the distance further increases, only one of the sub-pulses overlaps, giving rise to the last side maxima. The peak separation thus corresponds to the bunches inter-distance in the train. The Fourier transform of the autocorrelation function directly provides information on the resonant frequency of the emission and its bandwidth.

The frequency spectrum of the incident radiation pulse can then be obtained by inverse Fourier transforming $\delta(\tau)$.

The longitudinal form factor is then evaluated from the spectral angular distribution defined by Eq. (2) and integrated over the solid angle. From Eq. (3) it is clear that only the amplitude of the form factor can be retrieved, loosing any information on the phase. Therefore, a proper reconstruction procedure of the bunch profile needs additional manipulation based on Kramers-Kronig dispersion relation.[54,55] The accuracy of the method depends on the extension of the measured radiation spectrum.

IV. THE SPARC-LAB THz SOURCE

The SPARC THz source has been characterized under different beam charge values, bunch compression factors, and photoinjector laser pulse shapes, i.e., Gaussian single pulse or two and four pulses beam, in order to investigate different emission regimes, i.e., broad and narrow spectral bandwidth. The energy of the beam for the measurements presented here ranges between 100 MeV and 170 MeV depending on the RF compressor phase. The repetition rate is fixed at 10 Hz.

A. Broadband THz radiation

A broadband THz radiation spectrum has been obtained by sub-ps single bunches. Autocorrelation measurements of the CTR radiation generated by a 300 pC, 120 MeV beam have been performed for three different compression factors, defined as the ratio between the bunch length for 0° RF compressor phase (the electron beam is injected on the crest of the RF field in the first accelerating section) and the length at a given injection phase in the RF compressor. Figure 9 shows the effect of three different bunch lengths on the spectral extent: the shorter the pulse the higher the frequency content in the spectrum.

Figure 10 shows the CTR energy spectrum in μJ/THz, measured in case of similar bunch length but different charge, i.e., 500 pC (black squares) and 300 pC (red dots). The effect of the higher charge allows to exceed the 10 μJ/THz per pulse, confirming the great potential of a linac-based THz source. The drop below 300 GHz is due to the effect of the finite screen size, while above 3 THz it is mainly caused by the longitudinal extension of the bunch.

The knowledge of the coherent spectrum allows to get information on the beam longitudinal charge distribution, as
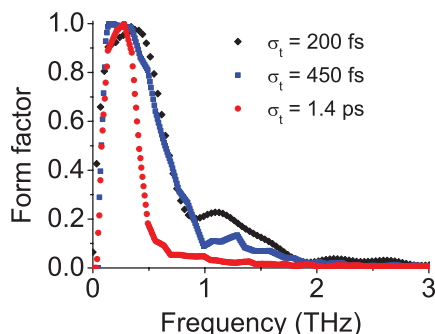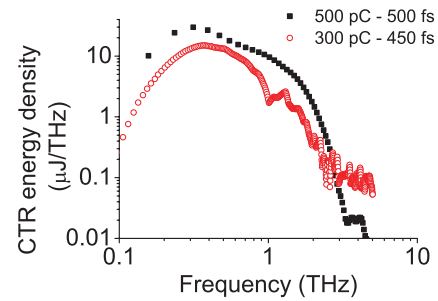
FIG. 10. CTR energy spectrum in μJ/THz, measured in case of a 500 pC, 500 fs (black squares), and 300 pC, 450 fs beam (red dots).

highlighted in Eq. (3). However, only the square of the Fourier transform of the longitudinal beam profile can be determined, preventing to retrieve any information on the phase. As discussed in Sec. III E, the procedure for the reconstruction of the bunch profile is based on Kramers-Kronig dispersion relation, allowing to determine the phase value consistent with the measured module. The accuracy of the method depends on the extension of the measured radiation spectrum, which is strongly affected by low and high frequency cut-off, introduced by the experimental apparatus. It is therefore mandatory the knowledge of the transfer function of the whole system, i.e., screen size, transmission of vacuum window, interferometer transfer function and the detectors frequency response.[21] All these arguments are taken into account to reconstruct the bunch profile, shown in the inset of Fig. 11, which provides a RMS bunch length of 0.45(0.050) ps. The bunch form factor extends up to 2 THz, in agreement with the measured bunch length.

B. Narrowband THz radiation

In this section, we report the measured THz spectra for different configurations of comb beams, i.e., two and four bunches train for different values of RF compressor phases. The production and transport, down to the linac exit, of a train of bunches with THz repetition rate has been successfully achieved,[24] even if challenging due to the high charge stored in each bunch, up to 200 pC in the two bunches train. On the other hand, as discussed in Sec. III D, the transport through the dogleg down to the THz station of such a longitudinally modulated beam can be dramatically affected by several parameters, e.g., beam energy spread, R_{56} of the

FIG. 9. Measured form factors for three different compression factors, corresponding to 200 fs, 450 fs, and 1.4 ps RMS bunch length.
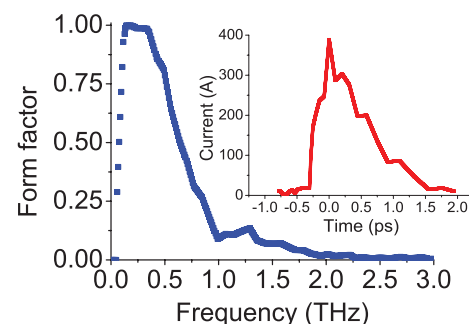
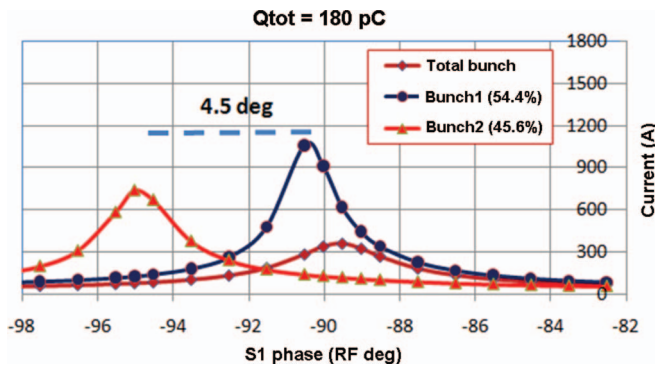FIG. 11. Measured form factor and retrieved bunch profile.

FIG. 12. Computed compression curves as function of the RF compressor phase for 180 pC total charge in the operating conditions of the COMB experiment at SPARC.

FIG. 13. Longitudinal phase space for low-charge (180 pC) compressed beam. (Left) compression, $-84°$. (Middle) maximum compression, $-90°$. (Right) over-compression, $-95.6°$. (Top) Measurements. (Bottom) Simulation.

beamline, etc., resulting in a degradation of the comb structure, and consequently in a widening of the THz emission bandwidth. We report here the experimental observations of this effect.

1. Two-bunches train

The dynamics of a beam generated by a "comb-like" laser pulse undergoing the RF compression is well described for the case of two-pulses in terms of the compression curves of the total beam and of the single bunches. Figure 12 shows the plot of the compression factor as function of the RF compressor phase for a 4.27 ps laser inter-pulses distance, a 520 fs RMS length for each pulse, and an amplitude of 54.4% in the head and 45.6% in the tail.

The distance between the two maxima of the single pulses curves increases with the charge, being proportional to the distance of the pulses at the entrance of the linac that, due to space charge, increases together with the total pulse length.

The total bunch compressor factor (purple dots in Fig. 12) increases up to a maximum value (around $-90°$ from the RF phase of maximum energy). Up to the phase of total bunch maximum compression, where the two sub-bunches overlap in time, their position is the same as that one at the cathode. Increasing further the compression phase, the sub-bunches invert their relative position, i.e., the bunch at the tail is now trailing the one at the head. Therefore, they start to separate in time and debunch each other. As also shown in Fig. 12, the dynamics of each sub-bunch is different: the first bunch reaches its maximum compression (black squares), while the second is still in a moderate compression regime (red triangles).

From the point of view of narrowband THz emission, we are interested in the so-called over-compression regime ($-95.6°$ from the on crest phase, Fig. 13, right), where the two bunches are well separated in time, i.e., 1 ps.

However, the beam has been experimentally characterized also in some other representative points of the compression curve. In particular, Fig. 13 shows the rotation of the beam longitudinal phase space during the beam compression for a total charge of 180 pC: passing from the compression region ($-84°$ from the on crest phase, Fig. 13, left) to the over-
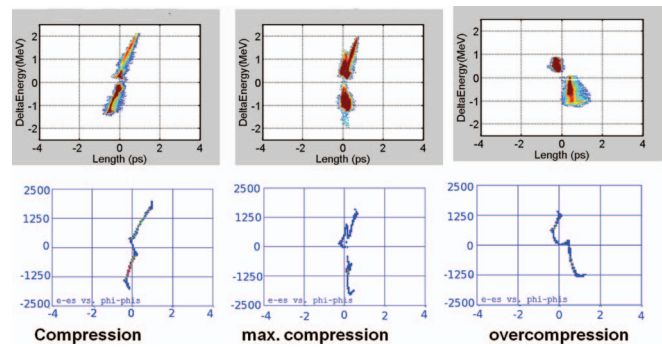
compression region ($-95.6°$ from the on crest phase, Fig. 13, right), the chirp of the total bunch changes sign. Under the transport through the dogleg, whose typical values are $R_{56} = -5$ mm with a $T_{566} = -95$ cm with a momentum spread of few % in the VB regime, the effective $\tilde{R}_{56}$ defined in Sec. III D may also change sign within the bunch train itself. Such a non-linear behavior might result in a further compression introduced by the dogleg, modifying the bunch train length, sub-bunches current, and bunch time separation. We observed this effect in simulations, by transporting the longitudinal phase space, for the $-84°$ case, from the end of the linac (Fig. 14, lower left) down to the THz station (Fig. 14, lower right), where one sub-bunch lengthens (Fig. 14, upper left), while the other is compressing (Fig. 14, upper right). In addition, this behavior has been also experimentally viewed through CTR autocorrelation measurements, providing the bunch form factor (Fig. 15). Indeed, in Fig. 15 only the $-84°$ case shows a clear peak around 1 THz, as expected by the simulated longitudinal phase space at the THz station. No effect of longitudinal modulation is instead observed for the other case and, in particular for the over-compression regime (blue dotted line and olive dashed-dotted line).
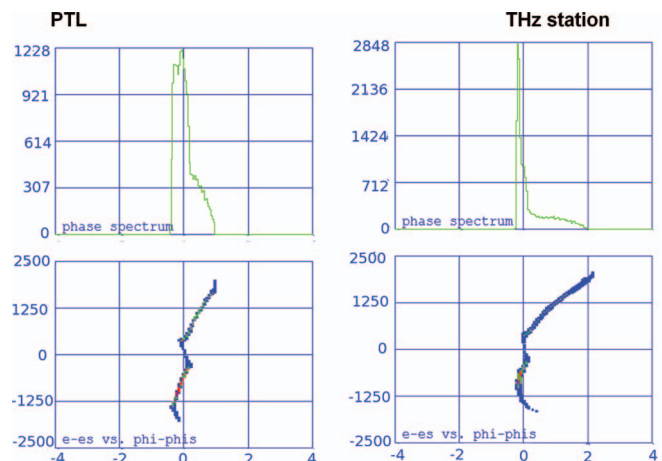

FIG. 14. Simulated longitudinal phase space, for the $-84°$ case, from the end of the linac (lower left) down to the THz station (lower right), where one sub-bunch lengthens (upper left), while the other is compressing (upper right).
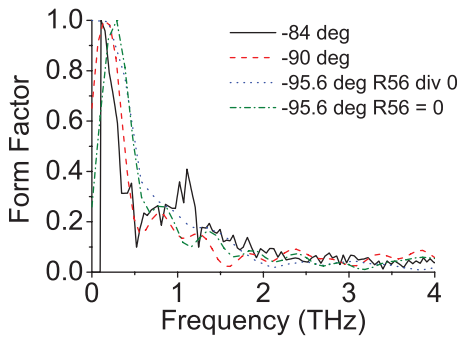
FIG. 15. Bunch form factors measured for different RF compressor phases: sub-compression (black solid line), maximum compression (red dashed line), over-compression (blue dotted line and olive dashed-dotted line). The last two curves are for different beam transport channel. 180 pC, 110 MeV beam.

2. Four-bunches train

For a four-bunches comb distribution, the proper pulse spacing and length for suitable narrowband THz generation has been found in the so-called deeply overcompression regime, in which all the sub-bunches are debunching at the exit of the linac, thus well separated in time.

The compression curve of the whole bunch is shown in Fig. 16; it reports the ratio between the bunch length at the maximum energy (i.e., no compression) with the bunch length for each injection phase in the first TW accelerating section (i.e., the RF compressor phase). Three different working conditions, namely, compression, over-compression, and deep over-compression, can be identified from the rotation of the phase space induced by the velocity bunching.[56] From the point of view of THz applications, which need a tunable and well defined bunch separation, the deep over-compression region is the most interesting one.

The start-to-end TSTEP simulations are in excellent agreement with the measured data and we can use them to investigate the beam dynamics. For example, Fig. 17 reports the compression curve for each of the four bunches as well as the whole bunch one.

Figure 17 also shows that the RF compressor phases can be used as a selector of the number of pulses in the final train. In the compression region, the bunch current ex-
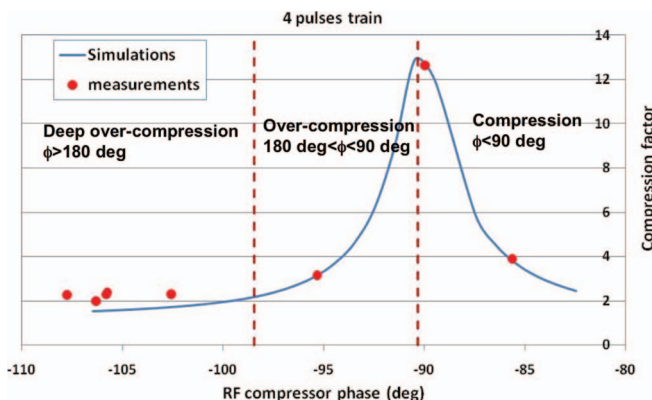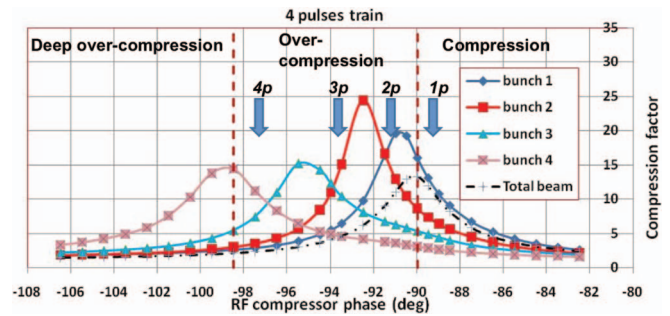

FIG. 17. Compression curve of each bunch of the comb beam (TSTEP simulation[53]).

hibits only a longitudinal modulation. By entering in the over-compression region, as soon as the first (head) sub-bunch is going through its maximum compression (diamond line) and before the maximum compression of the second sub-bunch (red square line), the current appears as two sub-bunches (*2p* label). By increasing the RF compressor phase, we can move towards a three sub-bunches train (*3p* label) and eventually towards a four sub-bunches train (*4p* label). Keeping in mind the description of the interferogram produced by such a longitudinal distribution, it is clear that, depending on the RF compressor phase, also the number of peaks in the measured interferogram can change.

As an example, we compare the CTR autocorrelation measurements, providing information on the THz spectrum, for two different deep over compression RF phases, i.e., −106° and −108° as indicated in Fig. 17, where the four bunches are well separated in time.

Figure 18(a) (red dots) shows the measured interferogram in case of −108° RF compression phase. In the same plot, it is reported the interferogram (blue dashed line) as expected from the longitudinal profile measured through the RFD (in the inset), giving a bunches time separation of 0.8 ps.

For such a longitudinal distribution, the interferogram is multipeaked (Fig. 18(a)), whose time distance corresponds to the separation of the bunches in the train (Fig. 18(b)). The retrieved form factor (Fig. 18(c)) is then peaked at the comb

FIG. 16. Whole bunch compression curve for the 4 sub-bunches train (TSTEP simulation,[53] measurements).
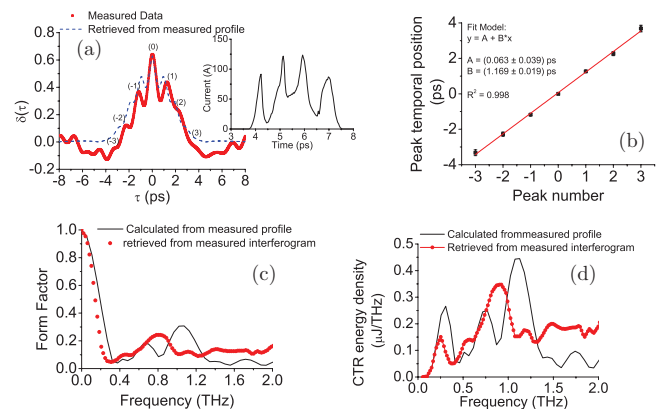

FIG. 18. (a) Multi-peak measured interferogram (red dots) and retrieved (solid blue line) from the measured longitudinal profile in the inset. (b) Time separation of the bunches in the train as function of the number of peaks in the interferogram. (c) Retrieved form factor peaked at the comb repetition frequency. (d) Measured CTR spectrum centered at 0.8 THz.
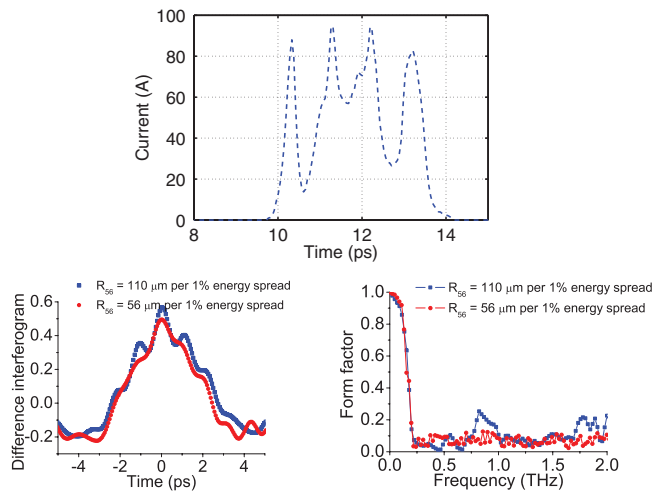
FIG. 19. (Top) Current profile measured through the RFD in case of $-106°$ RF compression phase. (Bottom left) Comparison between interferograms measured with the same beam parameters, but different settings of the dogleg transport beamline (R_{56}: 110 μm per 1% energy spread (blue squares) and 56 μm per 1% energy spread (red dots)). (Bottom right) Resulting form factors.

repetition frequency, whose bandwidth depends on both the modulation of the bunches in the train and their length. The measured spectrum is shown in Fig. 18(d)). A discrepancy in both interferograms and spectra, as calculated from the measured beam profile or retrieved from the Fourier transformation of the measured interferogram, is observed depending on the influence of the beam transport through a not well optimized dogleg beamline.

In order to highlight the effect of the beam transport through the dogleg, we also report the measurements in case of $-106°$ RF compression phase for different values of R_{56}. Figure 19 shows, for the same current profile measured through the RFD (Fig. 19, top), two sensitively different interferograms (Fig. 19, bottom left) depending on the beamline R_{56}: 110 μm per 1% energy spread (blue squares) and 56 μm per 1% energy spread (red dots). The effect on the form factor (Fig. 19, bottom right) is the showing up of a peak centered at the frequency corresponding to the time separation of the interferogram peaks.

C. Main features

Depending on the working point of the accelerator, the THz radiation can be tuned in order to optimize different characteristics. Namely, a single, sub-ps high brightness electron bunch is used to produce broadband, high power ra-

TABLE I. SPARC-LAB THz source performance: radiation parameters.

	Single bunch	Four-bunches per train
Energy per pulse (μJ)	>1	0.6 @ 1 THz
Peak power (MW)	100	3 @ 1 THz
Average power (W)	$1.8 \, 10^{-4}$	$6 \, 10^{-6}$
Electric field (kV/cm)	>100	>10
Pulse duration (fs)	<200	<100
Bandwidth (%)	...	<25

TABLE II. SPARC-LAB THz source performance: electron beam parameters.

	Single bunch	Four-bunches per train
Charge/bunch (pC)	500	50
Energy (MeV)	110	100
Bunch length (fs)	500	200
Rep. rate (Hz)	10	10

diation (see Sec. IV A); the required bunch length can be achieved with proper RF compression (the so called velocity bunching). A properly shaped bunch train has been used to drive narrowband THz radiation; by changing the sub-bunches spacing one can tune the central frequency of the radiation, as shown in Sec. IV B. As an example, we report in Table I the so far achieved THz radiation performances, in case of both a single-bunch and a four-bunch train whose parameters are presented in Table II.

V. CONCLUSIONS

The SPARC-LAB test facility is becoming a test bench for advanced high brightness beam applications, e.g., novel FEL schemes, advanced coherent THz generation, x-ray radiation, and plasma-based acceleration techniques. In particular, a review of the SPARC-LAB coherent THz radiation has been reported. Different THz emission regimes have been achieved by properly control pulse shaping, length, charge, and energy separation, therefore, by properly set the photoinjector parameters. Two main schemes are currently investigated, ultrashort single bunch and multi-bunches comb beams, to generate high energy per pulse, broad and narrow spectral bandwidth THz radiation, respectively.

ACKNOWLEDGMENTS

[1]Y.-S. Lee, *Principles of Terahertz Science and Technology* (Springer, 2008).
[2]B. Aune and R. H. Miller, SLAC-PUB Report No. 2393, 1979.
[3]B. E. Carlsten, Nucl. Instrum. Methods Phys. Res. A **285**, 313–319 (1989).
[4]L. Serafini and M. Ferrario, AIP Conf. Proc. **581**, 87 (2001).
[5]M. Ferrario *et al.*, Phys. Rev. Lett. **104**, 054801 (2010).
[6]M. Abo-Bakr *et al.*, Phys. Rev. Lett. **88**, 254801 (2002).
[7]A.-S. Mueller, Synchrotron Radiat. News **19**, 18 (2006).
[8]S. Lupi *et al.*, J. Opt. Soc. Am. B **24**(4), 959–964 (2007).
[9]D. Daranciang, J. Goodfellow, M. Fuchs, H. Wen, S. Ghimire, D. A. Reis, H. Loos, A. S. Fisher, and A. M. Lindenberg, Appl. Phys. Lett. **99**, 141117 (2011).
[10]M. C. Hoffmann, S. Schulz, S. Wesch, S. Wunderlich, A. Cavalleri, and B. Schimdt, Opt. Lett. **36**(23), 4473–4475 (2011).
[11]E. Chiadroni *et al.*, "The SPARC linear accelerator based terahertz source," Appl. Phys. Lett. (in press).
[12]Z. Wu, E. Adli, A. Fisher, H. Loos, and M. Hogan, in *Proceedings of the International Particle Accelerator Conference, IPAC2012, TUEPPB009, New Orleans, LA*, 2012.
[13]M. S. Sherwin *et al.*, "Opportunities in THz Science," Report of a DOE-NSF-NIH Workshop, 2004.
[14]J. van Tilborg, C. B. Schroeder, Cs. Tóóth, C. G. R. Geddes, E. Esarey, and W. P. Leemans, Opt. Lett. **32**(3), 313–315 (2007).

[15]Y. Shen, T. Watanabe, D. A. Arena, C.-C. Kao, J. B. Murphy, T. Y. Tsang, X. J. Wang, and G. L. Carr, Phys. Rev. Lett. **99**, 043901 (2007).

[16]Y. Shen, X. Yang, G. L. Carr, Y. Hidaka, J. B. Murphy, and X. Wang, Phys. Rev. Lett. **107**, 204801 (2011).

[17]J. G. Neumann, R. B. Fiorito, P. G. O'Shea, H. Loos, B. Sheehy, Y. Shen, and Z. Wu, J. Appl. Phys. **105**, 053304 (2009).

[18]S. G. Anderson *et al.*, Phys. Rev. ST Accel. Beams **8**, 014401 (2005).

[19]P. Piot *et al.*, Appl. Phys. Lett. **98**, 261501 (2011).

[20]J. Zhang, H. Deng, X. Lin, D. Dai, Q. Sun, S. Lu, T. Yu, H. Zhao, H. Yang, and Z. Dai, Nucl. Instrum. Methods Phys. Res. A **693**, 23–25 (2012).

[21]E. Chiadroni, TESLA-FEL Report No. 2006-09, 2006.

[22]J. van Tilborg *et al.*, Phys. Rev. Lett. **96**, 014801 (2006).

[23]A. Bacci *et al.*, in *Proceedings of the International Free Electron Laser Conference, FEL2011, THOB2, Shanghai, China*, 2011.

[24]M. Ferrario, D. Alesini, A. Bacci, M. Bellaveglia, R. Boni, M. Boscolo, P. Calvani, M. Castellano, E. Chiadroni, A. Cianchi *et al.*, Nucl. Instrum. Methods Phys. Res. A **637**, S43–S46 (2011).

[25]D. Alesini *et al.*, Nucl. Instrum. Methods Phys. Res. A **507**, 345–349 (2003).

[26]D. Alesini *et al.*, Laser Part. Beams **22**(3), 341–350 (2004).

[27]P. Valente *et al.*, Nucl. Instrum. Methods Phys. Res. A **653**(11), 42–46 (2011).

[28]A. Mostacci, M. Bellaveglia, E. Chiadroni, A. Cianchi, M. Ferrario, D. Filippetto, G. Gatti, and C. Ronsivalle, Phys. Rev. ST Accel. Beams **15**, 082802 (2012).

[29]D. Filippetto, M. Bellaveglia, M. Castellano, E. Chiadroni, L. Cultrera, G. Di Pirro, M. Ferrario, L. Ficcadenti, A. Gallo, G. Gatti *et al.*, Phys. Rev. ST Accel. Beams **14**(9), 092804 (2011).

[30]M. Ferrario *et al.*, Phys. Rev. Lett. **99**, 234801 (2007).

[31]E. Chiadroni *et al.*, in *Proceedings of the 35th International Conference of Infrared, Millimeter and THz waves (IRMMW-THZ 2010)*, 2010.

[32]E. Chiadroni *et al.*, J. Phys.: Conf. Ser. **357**, 012034 (2012).

[33]E. Chiadroni *et al.*, J. Phys.: Conf. Ser. **359**, 012018 (2012).

[34]M. Labat *et al.*, Phys. Rev. Lett. **107**, 224801 (2011).

[35]L. Giannessi *et al.*, Phys. Rev. Lett. **106**, 144801 (2011).

[36]L. Giannessi *et al.*, Phys. Rev. Lett. **108**, 164801 (2012).

[37]L. Giannessi *et al.*, Phys. Rev. ST Accel. Beams **14**, 060712 (2011).

[38]P. Antici, A. Bacci, C. Benedetti, E. Chiadroni, M. Ferrario *et al.*, J. Appl. Phys. **112**, 044902 (2012).

[39]L. Serafini *et al.*, in *Proceedings of the International Particle Accelerator Conference, IPAC2012, WEEPPB002, New Orleans, LA*, 2012.

[40]D. H. Martin and E. Puplett, Infrared Phys. **10**, 105–109 (1970).

[41]O. Limaj, A. Nucara, S. Lupi, M. Ortolani, A. Di Gaspare, E. Palange, and P. Carelli, Opt. Commun. **284**, 1690–1693 (2011).

[42]J. D. Jackson, *Classical Electrodynamics*, 3rd ed. (Wiley, 1995).

[43]M. Castellano, A. Cianchi, G. Orlandi, and V. A. Verzilov, Nucl. Instrum. Methods Phys. Res. A **435**, 297–307 (1999).

[44]S. Casalbuoni *et al.*, Phys. Rev. ST Accel. Beams **12**, 030705 (2009).

[45]A. P. Potylitsyn, Nucl. Instrum. Methods Phys. Res. B **145**(1–2), 169 (1998).

[46]J. S. Nodvick and D. S. Saxon, Phys. Rev. **96**, 180 (1954).

[47]R. Lai and A. J. Sievers, Nucl. Instrum. Methods Phys. Res. A **397**, 221–231 (1997).

[48]A. P. Potylitsyn, M. I. Ryazanov, M. N. Strikhanov, and A. A. Tischchenko, *Diffraction Radiation from Relativistic Particles* (Springer-Verlag, Berlin, 2010).

[49]Y. Shibata, T. Takahashi, T. Kanai, K. Ishi, M. Ikezawa, J. Ohkuma, S. Okuda, and T. Okada, Phys. Rev. E **50**, 1479 (1994).

[50]S. Casalbuoni, B. Schmidt, and P. Schmueser, TESLA Report No. 2005-15, 2005.

[51]M. Boscolo *et al.*, Nucl. Instrum. Methods Phys. Res. A **577**, 409–416 (2007).

[52]R. J. England *et al.*, Phys. Rev. ST Accel. Beams **8**, 012801 (2005).

[53]TSTEP is a derivative of PARMELA code; L. M. Young, PARMELA, Los Alamos National Laboratory report LA-UR-96-1835 (Revised April 22, 2003).

[54]F. Wooten, *Optical Properties of Solids* (Academic, New York, 1972).

[55]R. Lai and A. J. Sievers, Phys. Rev. E **50**, R3342 (1994).

[56]A. Mostacci *et al.*, in *Proceedings of the International Particle Accelerator Conference, IPAC11, THYB01*, San Sebastian (Spain), 2011.